Chalcogenide Letters Vol. 22, No. 8, August 2025, p. 665 - 677

3D/3D C-MoO_2/$Cd_{0.9}Zn_{0.1}S$ composite with an S-scheme electron transfer pathway enables highly efficient photocatalytic hydrogen evolution

C. M. Fu [a], M. Z. Ge [b] , X. Q. Zhang [c], W. Yan [c,*]

[a] *School of Mechanical Engineering and Transportation, Changzhou Vocational Institute of Industry Technology, Changzhou, 213164, P. R China,*

[b] *School of Materials Engineering, Jiangsu University of Technology, Changzhou, 213001, P. R China*

[c] *School of Physics and Electronic Engineering, Jiangsu University, Zhenjiang, 212013, P. R. China*

Constructing heterojunctions represents a crucial strategy for enhancing semiconductor photocatalysts. In this study, the C-MoO_2/$Cd_{0.9}Zn_{0.1}S$ S-scheme heterojunction composite was successfully fabricated through a self-assembly approach. XPS analysis confirmed the spontaneous transfer of intrinsic electrons from $Cd_{0.9}Zn_{0.1}S$ to C-MoO_2 in the dark, establishing an internal electric field at the C-MoO_2/$Cd_{0.9}Zn_{0.1}S$ interface. Under visible light irradiation, the C-MoO_2/$Cd_{0.9}Zn_{0.1}S$ composite exhibited significantly enhanced hydrogen evolution activity, achieving a 6.3-fold improvement compared to pristine $Cd_{0.9}Zn_{0.1}S$. PL, TRPL, and electrochemical measurements collectively demonstrated that the incorporation of C-MoO_2 effectively suppressed the recombination of photogenerated electrons in $Cd_{0.9}Zn_{0.1}S$. The outstanding photocatalytic performance and improved charge carrier separation efficiency can be attributed to the S-scheme heterojunction configuration, which facilitates efficient electron transfer from $Cd_{0.9}Zn_{0.1}S$ to C-MoO_2. This work provides valuable experimental guidance for designing and constructing S-scheme heterojunction photocatalytic systems for solar hydrogen production.

(Received April 18, 2025; Accepted August 1, 2025)

Keywords: $Cd_{0.9}Zn_{0.1}S$, C doped with MoO_2, S-scheme heterojunction, Photocatalytic

1. Introduction

Hydrogen has garnered global attention due to its high energy content, pollution-free byproducts [1-3]. Currently, there are numerous methods for hydrogen production, with photocatalytic decomposition of water being a particularly promising approach [4-5]. This method is simple, cost-effective, environmentally friendly. Among these, metal sulfides have attracted significant interest due to their strong absorption of visible light and low band gaps [6-7]. Cadmium sulfide (CdS) is a common semiconductor photocatalyst within the metal sul-fide category, but it suffers from issues such as poor photocatalytic stability [8-9]. In recent years, researchers have turned to forming solid solutions by adding other metals, such as zinc, to CdS (forming $Cd_{1-x}Zn_xS$),

* Corresponding author: yanwei_jsdx@163.com

https://doi.org/10.15251/CL.2025.228.665

which can enhance stability while improving perfor-mance [10-11]. Although these synthetic solid solutions outperform pure CdS, they still face the challenge of rapid carrier recombination. Previous studies have demonstrated that constructing heterojunctions can effectively enhance charge carrier separation while simultaneously optimizing light absorption properties and modulating redox potentials [12-14].

Staggered heterojunctions have garnered considerable research interest due to their exceptional charge transfer and separation capabilities [15-16]. Unlike type-I (nested) heterojunctions where carriers are confined, staggered heterojunctions enable spatial separation of electrons and holes, thereby significantly enhancing photocatalytic performance. Conventional type-II heterojunctions represent the most common staggered configuration, but their photocatalytic activity remains limited as both electrons and holes are restricted to lower energy states. The emerging S-scheme heterojunction has attracted substantial attention because it maintains charge carriers with stronger redox potentials. Importantly, oxidation photocatalyst (OP) has a lower Fermi level than the reduction photocatalyst (RP) [16]. Upon contact between OP and RP, intrinsic electrons from RP spontaneously transfer to OP across their interface, creating a built-in electric field at the interface. Under illumination, photogenerated electrons follow a reverse migration path against the intrinsic electron flow. Electrons and holes generated by photon absorption become spatially separated. Therefore, the S-scheme heterojunction photocatalytic system can effectively facilitate the separation of photogenerated carriers in $Cd_{1-x}Zn_xS$ while preserving its strong redox capability.

In this study, Solvothermal synthesis was conducted separately to prepare C-doped MoO_2 and $Cd_{0.9}Zn_{0.1}S$, and the C-MoO_2/$Cd_{0.9}Zn_{0.1}S$ S-scheme heterojunction photocatalyst was fabricated by simply loading C-MoO_2 onto $Cd_{0.9}Zn_{0.1}S$ through mechanical stirring. The construction of the S-scheme heterojunction not only effectively promotes interfacial charge transfer, but also broadens the light absorption range compared to individual $Cd_{0.9}Zn_{0.1}S$ and C-MoO_2 components. In photocatalytic hydrogen evolution tests, the optimized C-MoO_2/$Cd_{0.9}Zn_{0.1}S$ composite exhibited approximately 6.3 times higher activity than pristine $Cd_{0.9}Zn_{0.1}S$. The synergistic enhancement effect of C-MoO_2 on the catalytic activity of $Cd_{0.9}Zn_{0.1}S$ was systematically investigated, and a plausible mechanism was proposed. This work provides valuable insights for designing high-performance photocatalytic hydrogen evolution catalysts through S-scheme heterojunction engineering.

2. Materials and methods

2.1. Materials

Cadmium acetate ($Cd(CH_3CO_2)_2$, ≥ 99.8%), Zinc acetate ($(CH_3COO)_2Zn$, ≥ 99.5%), Ammonium molybdate ($(NH_4)_6Mo_7O_{24}\cdot 4H_2O$, 99.8%), Thioacetamide (CH_3CSNH_2, 99.8%, TAA), glucose ($C_6H_{12}O_6$, ≥99.8%), ethylenediamine ($C_2H_8N_2$, ≥99.8%).

2.2. Synthesis of $Cd_{0.9}Zn_{0.1}S$ nanorods (NRs)

$Cd_{0.9}Zn_{0.1}S$ nanorods (NRs) are synthesized by the following steps: A liquid mixture consisting of cadmium acetate (2.39 g) and zinc acetate (0.22 g) in a mixed solvent of water (15 mL) and ethylamine (15 mL) was continuously stirred to obtain a uniform mixture. Then, under rapid agitation, TAA (0.98 g) is added to the above solution. The resulting solution was then transferred

into a 50 mL Teflon-lined autoclaves and heated at 220 ℃ for 24 h. Then naturally cooled, the yellow samples was washed with 3 water and 3 alcohol and then transferred to the vacu-um oven at 80 °C overnight. Yellow $Cd_{0.9}Zn_{0.1}S$ powder was obtained by grinding.

2.3. Synthesis of C doped with MoO_2 Nanoparticles (NPs)

C-MoO_2 Nanoparticles (NPs) are synthesized by the following steps: molybdate acid (1 g) in 50 ml water, followed by the addition of a specified amount of glucose under continuous stirring. The resulting solution was transferred into the same type of autoclave (as used for $Cd_{0.9}Zn_{0.1}S$ synthesis) at 180 °C for 12 h. Then naturally cooled, the black samples was washed with 2 water and 2 alcohol and then transferred to the vacuum oven at 70 °C. Black C-MoO_2 powder was obtained by grinding.

2.4. Synthesis of C-MoO_2/$Cd_{0.9}Zn_{0.1}S$

C-MoO_2 (1 mg, 3 mg, 5 mg, 7 mg, 9 mg) were uniformly dispersed in 50 ml water by ul-trasonic wave. Then 100 mg of $Cd_{0.9}Zn_{0.1}S$ ultrasound was added to evenly disperse them. C-MoO_2/$Cd_{0.9}Zn_{0.1}S$ is formed by electrostatic self-assembly after stirring for 12 h.

The sample was repeatedly washed with water and ethanol prior to vacuum drying. Grinding into powder corresponding named (1%, 3%, 5%, 8%, 9%) MCZS.

2.5. Characterization

The samples were measured by X-ray diffraction (XRD) with D/Max-2550 diffractometer. The Raman measurement of the sample was performed by DXR spectrometer. The sample morphology was characterized by scanning electron microscopy (SEM, JSM-7001F) and transmission electron microscopy (TEM, JEM-2100). Optical absorption properties were analyzed with a UV-2550. The X-ray photoelectron spectroscopy (XPS) measurement of the sample was performed by PHI ESCA-5000C spectrometer. F-7000(Hitachi) fluorescence spectrophotometer was used to measure the pho-toluminescence (PL) of the sample, and the excitation wavelength was 400nm. The time-resolved photoluminescence decay spectrum (TRPL) of the sample was measured using Edinburgh FI/FSTCSPC 920 spectrophotometer. The lectrochemical measurements of the sample was performed by CHI660D.

2.6. Photocatalytic performance measurements

A PerfectLight xenon lamp with a cut 420 nm filter was selected as the light source, and a 150 ml three-port flask was used as the hydrogen production reaction flask. Sample prep-aration steps: First, 20 mg of the prepared sample was weighed and 80 ml lactic acid solu-tion containing 10% volume was added into the reaction flask. After that, the samples were dispersed in the lactic acid solution more evenly by ultrasonic and stirring treatment, and were purged with N_2 for 15 min. Gas samples (0.4 mL) were periodically withdrawn from the glass flask at 1-hour intervals and injected into a gas chromatograph (GC-8A) for hydrogen quantification.

The apparent quantum yield (AQY) is as follows:

$$\mathrm{AQY} = \frac{amount\ of\ released\ hydrogen\ molecules\ in\ unit\ time \times 2}{number\ of\ incident\ photons\ in\ unit\ time} \times 100\%$$

3. Results and discussion

We conducted X-ray diffraction (XRD) analysis on both the pure and composite samples. The diffraction peaks of the synthesized pure phase $Cd_{0.9}Zn_{0.1}S$ are primarily at 24.8°, 25.8°, 27.7°, 36.5°, 44.7°, 47.8°, and 53.8°, which correspond to the diffraction peaks of $Cd_{0.9}Zn_{0.1}S$ reported in the literature (JCPDS No. 00-040-0384). The diffraction peaks of the pure phase C-MoO_2 are mainly located at 25.5°, 36.5°, and 54.2°, which are attributed to the diffraction peaks of MoO_2 (JCPDS No. 032-0671) (Figure 1a). The XRD peaks of the pure phases $Cd_{0.9}Zn_{0.1}S$ and C-MoO_2 indicate good crystallinity. The composite samples of C-MoO_2-modified $Cd_{0.9}Zn_{0.1}S$ show similar patterns. This simi-larity may be due to the close diffraction peaks of pure C-MoO_2 to those of $Cd_{0.9}Zn_{0.1}S$ and the relatively low content of C-MoO_2 in the composite material [17-20]. This is further supported by the XRD patterns of MCZS with different composite ratios (Figure 1b), where the introduction of $Cd_{0.9}Zn_{0.1}S$ does not alter the diffraction peaks. Based on our previous work, it can be conclusively demonstrated that carbon is incorporated into MoO_2 via substitutional doping [12].

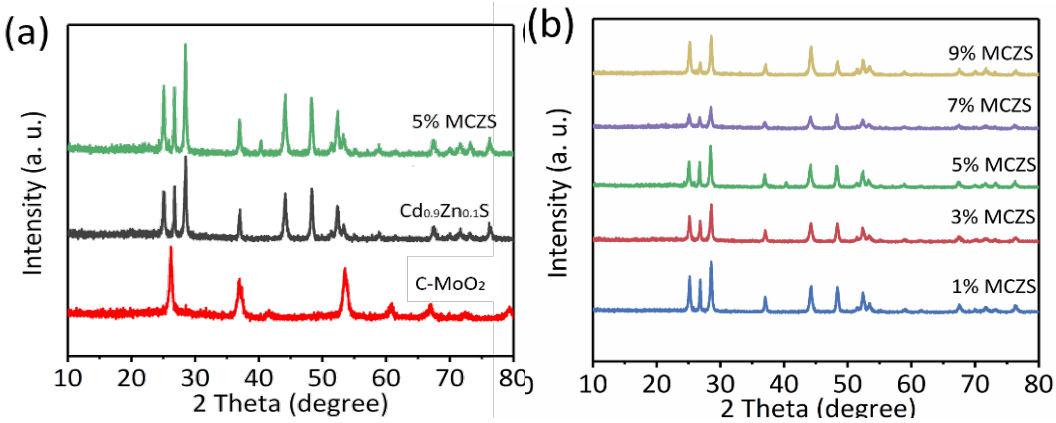

Fig. 1. XRD patterns of (a) C-MoO_2, $Cd_{0.9}Zn_{0.1}S$ and 5% MCZS nanocomposite; (b) XRD patterns of 1%-9% MCZS nanocomposite.

Figure 2 presents the morphological characterization results of the materials [21-25]. Figure 2a shows pure $Cd_{0.9}Zn_{0.1}S$. It can be seen from the figure that $Cd_{0.9}Zn_{0.1}S$ is rod-shaped with a diameter of about 100 nm and has good dispersion. Figure 2b shows pure C-MoO_2, from which it can be seen that C-MoO_2 is irregular particles. Figure 2c is a composite sample, which shows that the structure of $Cd_{0.9}Zn_{0.1}S$ does not change significantly after loading the additive C-MoO_2. It can be seen more clearly from Figure 2d that Co-catalyst C-MoO_2 particles are loaded on $Cd_{0.9}Zn_{0.1}S$. The TEM and HAADF-STEM characterization results of the 5% MCZS sample are presented in Figure 3a-i. As can be seen from TEM images, $Cd_{0.9}Zn_{0.1}S$ is a solid bar with a diameter of about 100 nm (Figure 3a). C-MoO_2 particles are about 50 nm in size and attach to $Cd_{0.9}Zn_{0.1}S$ (Figure 3b). The measured lattice fringes of 0.17 nm correspond to the (220) plane of C-MoO_2, while the 0.33 nm spacing matches the (002) plane of $Cd_{0.9}Zn_{0.1}S$ (Figure 3c) [5, 26]. The results of TEM test prove the successful construction of C-MoO_2/$Cd_{0.9}Zn_{0.1}S$ heterojunction. EDX mappings of HAADF-STEM (Figure 3d-i) depict the distribution of ele-ments Cd, Zn, S, Mo, O and C. The successful doping of carbon into MoO_2 was confirmed.

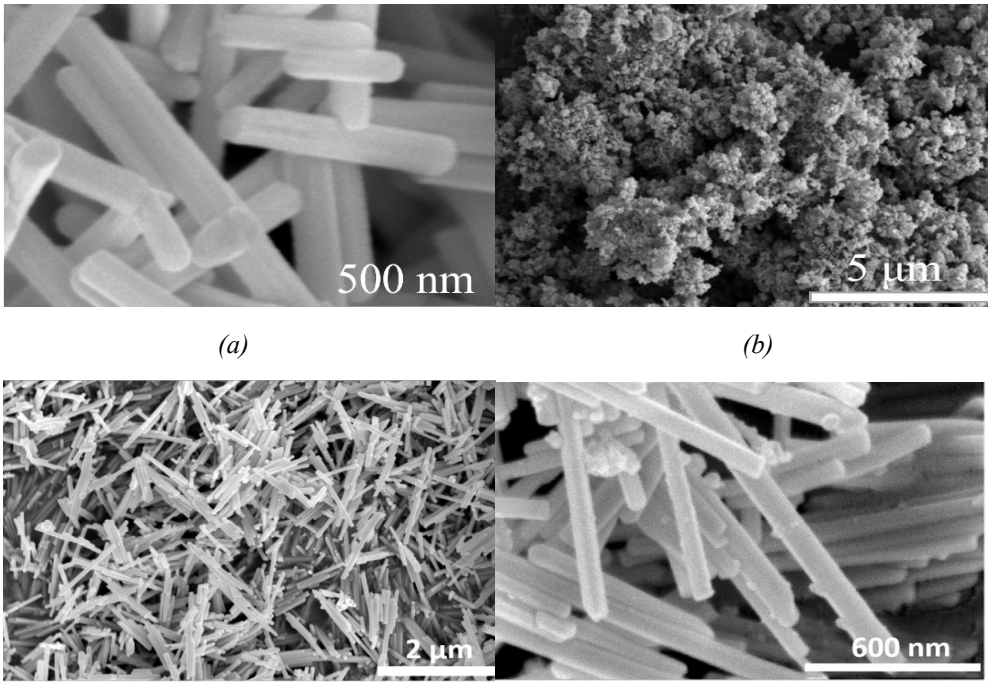

(a) *(b)*

(c) *(d)*

Fig. 2. SEM patterns of (a) pure $Cd_{0.9}Zn_{0.1}S$;(b) pure C-MoO_2; (c-d) 5% MCZS.

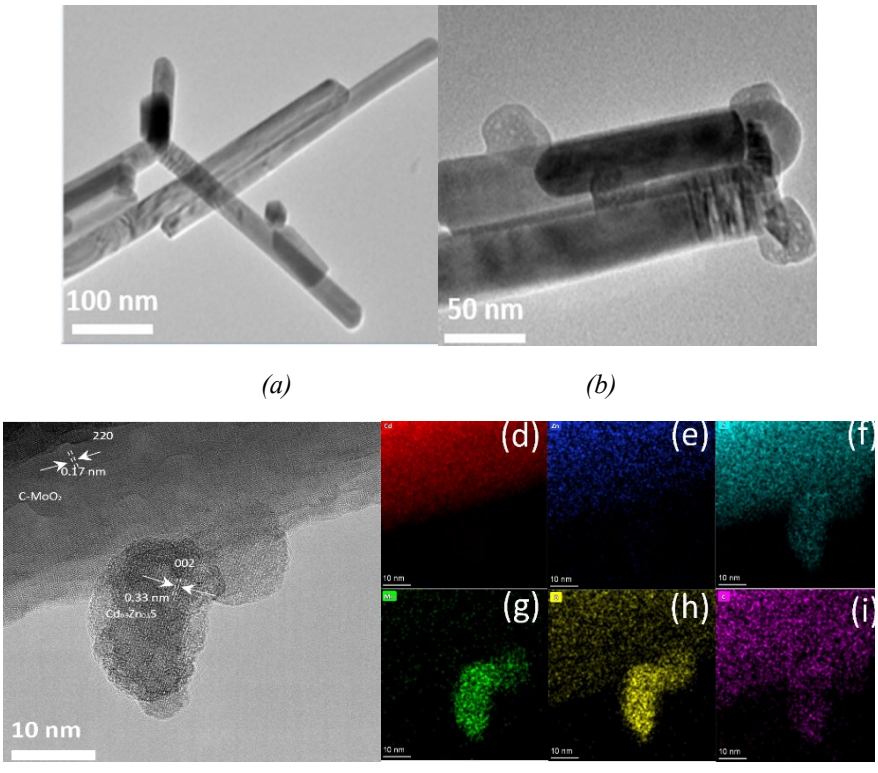

(a) *(b)*

(c)

Fig. 3. TEM images of (a) CdZnS, (b) 5% MCZS; HRTEM image of (e) 5% MCZS composite; elemental mapping images of (d-i) 5% MCZS composite.

Figure 4a demonstrates the light absorption capability of the sample [27-30]. The pure $Cd_{0.9}Zn_{0.1}S$ sample has an obvious absorption band edge at approximately 520 nm. The composite sample exhibits optical absorption up to approximately 520 nm, which is similar to that of the pure sample. However, in the region above 520 nm, the composite sample exhibits obvious light absorption. The incorporation of black C-MoO_2 enhances the tail absorption of the composite material. With the growing amount of C-MoO_2, the tail absorption strength of the composite samples will in-crease. The absorption edge of $Cd_{0.9}Zn_{0.1}S$ is approximately 520 nm, and the corresponding band gap is approximately 2.33 eV (Figure 5b). Combining Mott-Schottky plots (Figure 5c) with the follow-ing formulas [31]:

$$E_{fb}(vs\ NHE, PH = 0) = E_{fb}(vs, Ag/AgCl) + 0.059 \times pH + 0.179 \quad (1)$$

$$E_{CBM}(vs\ NHE) = E_{fb}(vs\ NHE, PH = 0) - 0.3 \quad (2)$$

conductive band (CB) values of $Cd_{0.9}Zn_{0.1}S$ can be calculated as -0.24 eV. The band structure of C-MoO_2 refers to previous work.

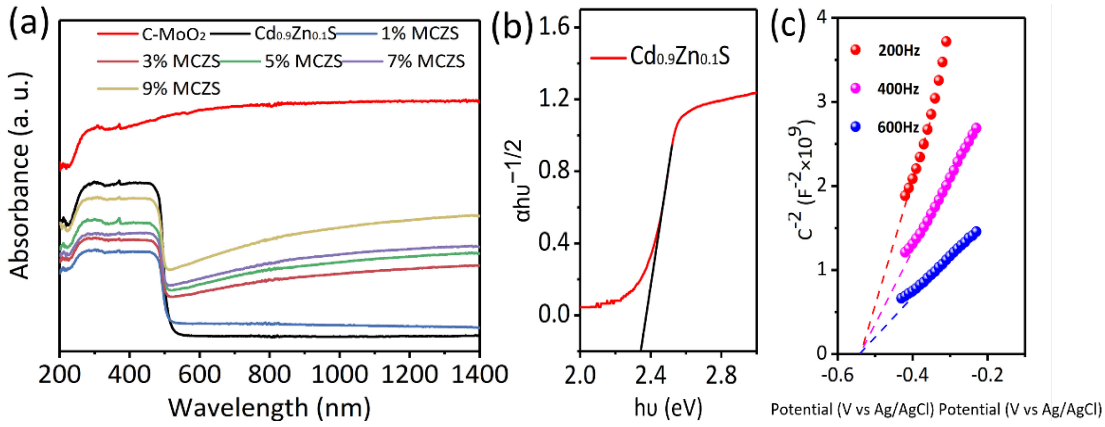

Fig. 4. (a) ultraviolet-visible absorption spectra; (b) band gap of $Cd_{0.9}Zn_{0.1}S$, (c) Mott-Schottky plots of $Cd_{0.9}Zn_{0.1}S$.

The surface structures and electronic states of pristine C-MoO_2, $Cd_{0.9}Zn_{0.1}S$, and their composite were analyzed by XPS [32-35]. In the Cd 3d of $Cd_{0.9}Zn_{0.1}S$, Cd $3d_{5/2}$ (404.73 eV) and $3d_{3/2}$ (411.45 eV) can be observed (Figure 5b). In the Zn 2p XPS spectrum of $Cd_{0.9}Zn_{0.1}S$, Zn $2p_{3/2}$ (1022.47 eV) and Zn $2p_{1/2}$ (1043.59 eV) can be observed (Figure 5c). In the S 2p of $Cd_{0.9}Zn_{0.1}S$, S $2p_{3/2}$ (161.02 eV) and S $2p_{1/2}$ (162.11 eV) can be observed (Figure 5d) [5]. Compared with the Cd 3d, Zn 2p, S 2p of pure $Cd_{0.9}Zn_{0.1}S$, the peaks of the composite samples all shift to higher binding energies, indicating electron redistribution between C-MoO_2 and $Cd_{0.9}Zn_{0.1}S$. The electrons on $Cd_{0.9}Zn_{0.1}S$ transferred to C-MoO_2. In Figure 5e, the characteristic peaks of pristine C-MoO_2 can be observed, including Mo^{3+} $3d_{5/2}$ (229.40 eV) and $3d_{3/2}$ (231.43 eV), Mo^{4+} $3d_{5/2}$ (229.98 eV) and $3d_{3/2}$ (234.40 eV), as well as Mo^{6+} $3d_{5/2}$ (232.77 eV) and $3d_{3/2}$ (236.02 eV) [36]. The existence of the Mo^{6+}

oxidation state in the C-MoO_2 material may be due to surface oxidation in the air, while the presence of the low oxidation state Mo^{3+} may be attributed to the existence of carbon materials. Only Mo^{4+} ($3d_{5/2}$ at 231.86 eV and $3d_{3/2}$ at 234.02 eV) could be observed in the composite sample's Mo 3d XPS spectrum, which may be due to the strong interference of the S 2s peak at 224 eV. Figure 5f shows the O 1s XPS spectrum, and the peaks at 530.40 eV in the figure correspond to the oxygen band of Mo-O-Mo (lattice oxygen). The peak at 531.67 eV corresponds to O in H_2O [37-40].

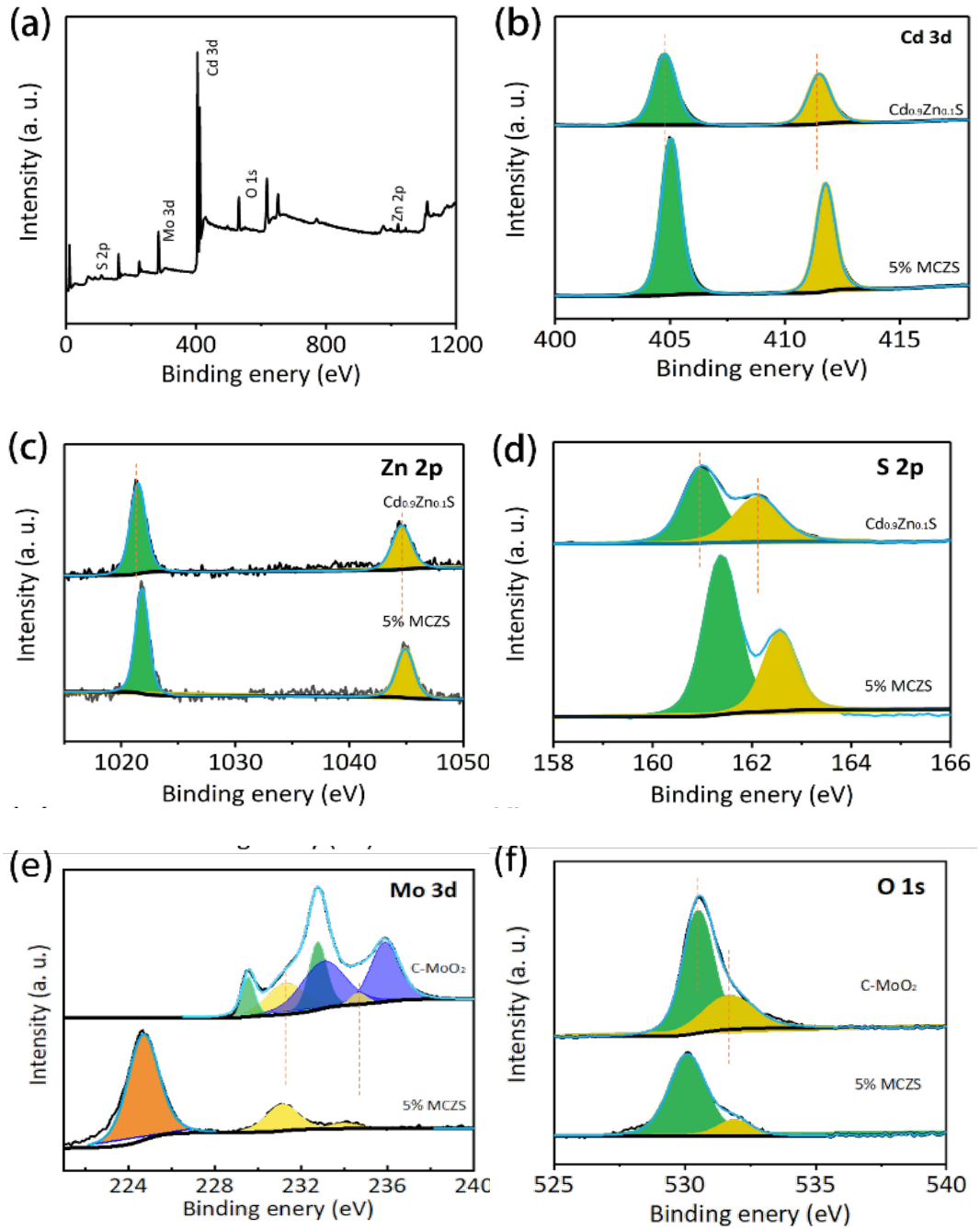

Fig. 5. (a) XPS survey spectrum; (b) Cd 3d, (c) Zn 2p, (d) S 2p, (e) Mo 3d, and (f) O 1s of $Cd_{0.9}Zn_{0.1}S$, C-MoO_2, and 5% MCZS composite.

The transfer, separation, and recombination processes of photogenerated carriers were measured using photocurrent (i-t) and impedance (EIS) [41-44]. The photocurrent density of the composite sample is significantly enhanced relative to the pure phase, indicating that the photoelectrons generated by $Cd_{0.9}Zn_{0.1}S$ are more inclined to transfer to C-MoO_2, thereby achieving better electron-hole separation and generating a higher photocurrent (Figure 6a). Figure 6b displays the test results of EIS. The relative arc size of the test electrodes for the three materials is in the order of $Cd_{0.9}Zn_{0.1}S$ > 5% MCZS (assuming 'MCZS' is a shorthand for the composite material), and these results are consistent with the i-t test results. It is demonstrated that the addition of C-MoO_2 can reduce the electron transfer resistance of $Cd_{0.9}Zn_{0.1}S$ and promote the separation of interfacial charges.

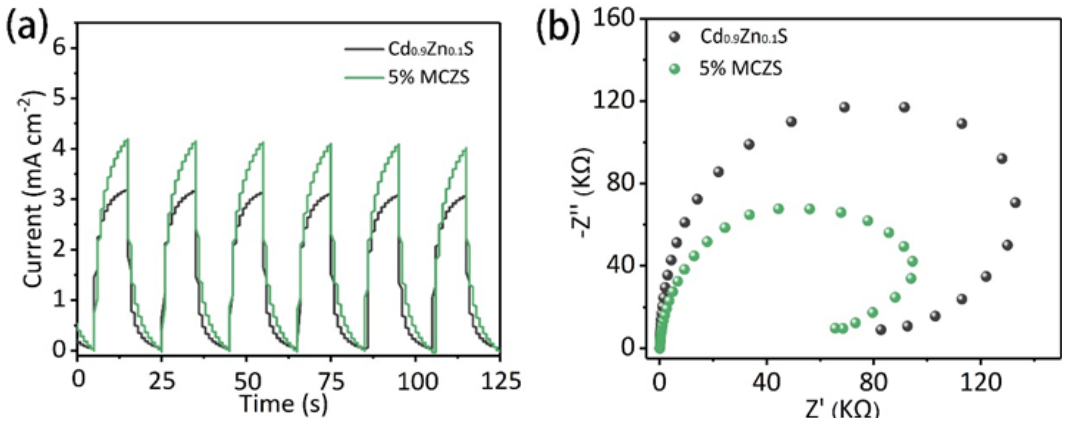

Fig. 6. (a) i-t, (b) EIS of $Cd_{0.9}Zn_{0.1}S$ and 5% MCZS samples under full light irradiation.

Photoluminescence (PL) spectroscopy is an effective means to study the effective separation of charges in photocatalysts [45]. The photoluminescence spectrum of pure $Cd_{0.9}Zn_{0.1}S$ ex-hibits a broad absorption peak at 537 nm. The emission peak intensity of 5% MCZS com-posites is significantly weaker than that of pure $Cd_{0.9}Zn_{0.1}S$, indicating that the effective separation of charge is enhanced and the recombination is delayed at the interface between C-MoO_2 and $Cd_{0.9}Zn_{0.1}S$ (Figure 7a). This allows more electrons to participate in the reaction. The photophysical behavior of photoelectric charges is further analyzed by time-resolved photoluminescence (TRPL) (Figure 7b). It can be observed from the figure that 5% MCZS composites have a longer average decay time (in nanoseconds, ns) than pure $Cd_{0.9}Zn_{0.1}S$, which suggests that the photogenerated carriers in the 5% MCZS composite material can persist longer and have more opportunities to participate in the reaction.

Figure 8a shows the C-MoO_2 synthesized under different glucose dosage. Then, a certain amount of C-MoO_2 was combined with a certain amount of $Cd_{0.9}Zn_{0.1}S$ to improve the hydrogen production performance. The results showed that the best effect was achieved when the amount of reducing agent glucose was 140 mg. Figure 8b shows the hydrogen production performance of C-MoO_2 synthesized from 140 mg of glucose and different amounts of $Cd_{0.9}Zn_{0.1}S$. The results showed that the performance was highest when the C-MoO_2 content was 5%. AQY testing showed that 5% MCZS could achieve 28% under 360 nm light exposure (Figure 8c). After that, we conducted a cycle performance test on the 5% MCZS sample. As shown in Figure 8d, when 5% C-MoO_2 is added to $Cd_{0.9}Zn_{0.1}S$, the performance is stable, indicating that the addition of C-MoO_2 can improve the stability of $Cd_{0.9}Zn_{0.1}S$.

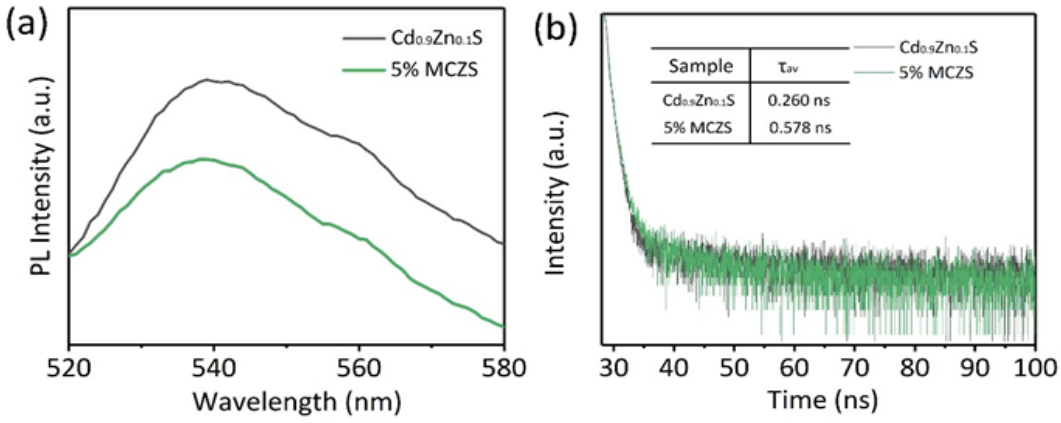

Fig. 7. (a) PL and (b) TRPL spectroscopy of $Cd_{0.9}Zn_{0.1}S$ and 5% MCZS.

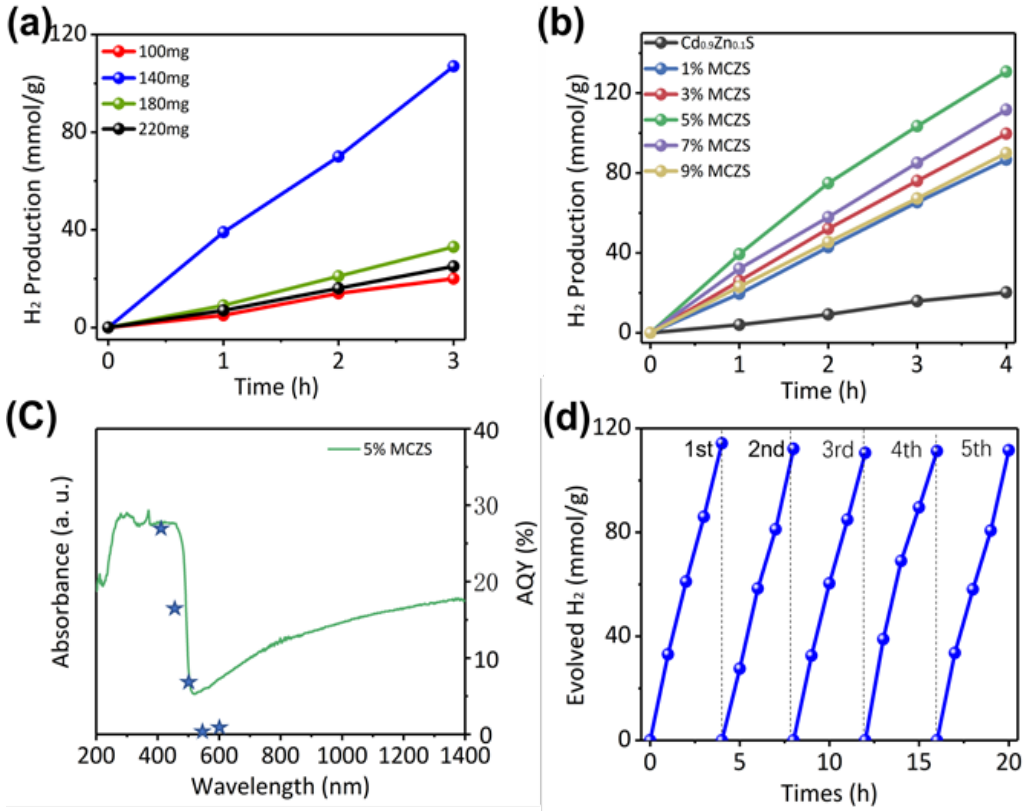

Fig. 8. (a) Photocatalytic hydrogen production activity of C-MoO_2 synthesized by different dosage of glucose combined with a certain amount of $Cd_{0.9}Zn_{0.1}S$; (b) The dosage of glucose was 140 mg of synthesized C-MoO_2, photocatalytic hydrogen production activity of a certain amount of $Cd_{0.9}Zn_{0.1}S$ combined with different amounts of C-MoO_2; (c) the AQY (apparent quantum yield) test results; (d) recycling stability for sample 5% MCZS.

Based on these findings, we propose a possible photocatalytic mechanism, as shown in Figure 9. Under illumination, the conduction band (CB) of $Cd_{0.9}Zn_{0.1}S$ generates electrons, while the valence band (VB) generates holes. Electrons can participate in the reduc-tion of H^+, while holes are consumed by the sacrificial agent lactic acid. However, the pristine $Cd_{0.9}Zn_{0.1}S$ exhibits relatively low hydrogen evolution performance due to its poor charge carrier separation efficiency.

After the addition of C-MoO_2, XPS test results indicate that the intrinsic electrons of $Cd_{0.9}Zn_{0.1}S$ spontaneously flow toward C-MoO_2, forming an internal electric field directed from $Cd_{0.9}Zn_{0.1}S$ to C-MoO_2. When the C-MoO_2/$Cd_{0.9}Zn_{0.1}S$ catalyst is irradiated by light, the CB photoelectrons of C-MoO_2 recombine with VB holes of $Cd_{0.9}Zn_{0.1}S$ under the action of internal electric field. The photogenerated electrons in $Cd_{0.9}Zn_{0.1}S$ can reduce H^+ to H_2, while the holes left by the VB electron transition in C-MoO_2 are consumed by sacrificial agents. This forms an S-shaped electron transfer pathway, enhancing the carrier separation efficiency of the individual components $Cd_{0.9}Zn_{0.1}S$ and C-MoO_2, improving the performance of photocatalytic.

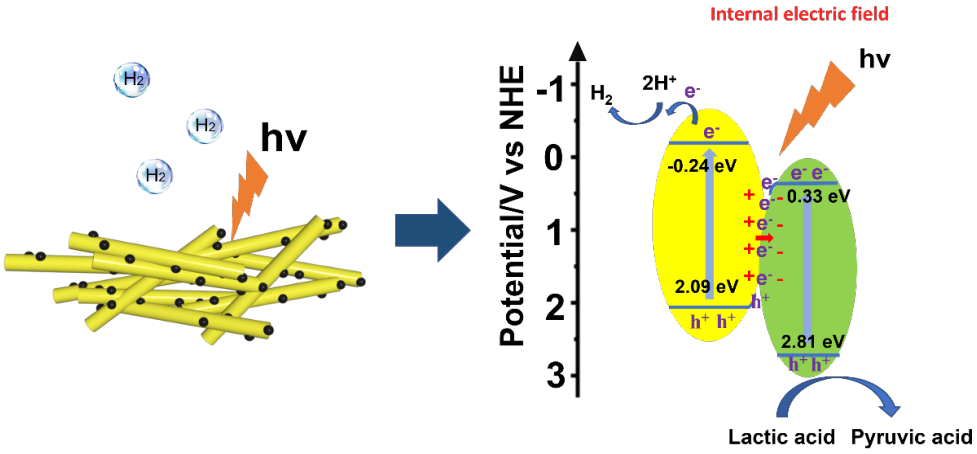

Fig. 9. The mechanism diagram of photocatalytic hydrogen production by 5% MCZS.

5. Conclusions

In summary, this study successfully synthesized C-doped MoO_2 and $Cd_{0.9}Zn_{0.1}S$ catalysts simultaneously via a one-step hydrothermal method, followed by the preparation of C-MoO_2/$Cd_{0.9}Zn_{0.1}S$ composite through simple mechanical mixing. XRD and Raman analyses confirmed the successful formation of C-doped MoO_2 and the composite materials. XPS characterization revealed the transfer of intrinsic electrons from $Cd_{0.9}Zn_{0.1}S$ to C-MoO_2, establishing a built-in electric field. UV-Vis spectroscopy demonstrated that the incorporation of C-MoO_2 significantly enhanced the light absorption capacity of $Cd_{0.9}Zn_{0.1}S$. The constructed S-scheme heterojunction in C-MoO_2/$Cd_{0.9}Zn_{0.1}S$ remarkably improved the photocatalytic hydrogen evolution performance compared to pristine $Cd_{0.9}Zn_{0.1}S$. With a 5% loading of C-MoO_2 cocatalyst, the composite achieved an optimal hydrogen production rate of 40 mmol/h, representing a 6.3-fold enhancement over the pure $Cd_{0.9}Zn_{0.1}S$. The comprehensive investigation demonstrates that the engineered S-scheme heterojunction effectively promotes light harvesting and charge carrier separation, thereby significantly boosting the photocatalytic efficiency.

References

[1] Wei W, Tian Q, Sun H, et al., Appl. Catal. B-Environ, 2020, 260: 118153; https://doi.org/10.1016/j.apcatb.2019.118153

[2] Liang J, Li H, Chen L, et al., Ind. Crops Prod., 2023, 193: 116214; https://doi.org/10.1016/j.indcrop.2022.116214

[3] Yan W, Xu Y, Hao S, et al., Inorg. Chem., 2022, 61(11): 4725-4734; https://doi.org/10.1021/acs.inorgchem.2c00045

[4] Ahmad M, Quan X, Chen S, et al., Appl. Catal. B-Environ, 2021, 283: 119601; https://doi.org/10.1016/j.apcatb.2020.119601

[5] Guo X, Guo P, Wang C, et al., Chem. Eng. J., 2020, 383: 123183; https://doi.org/10.1016/j.cej.2019.123183

[6] Yao L, Wei D, Ni Y, et al., Nano Energy, 2016, 26: 248-256; https://doi.org/10.1016/j.nanoen.2016.05.031

[7] Bi X, Li L, Luo L, et al., Food Chem., 2022, 385: 132657; https://doi.org/10.1016/j.foodchem.2022.132657

[8] Zhou P, Zhang Q, Chao Y, et al., Chem, 2021, 7(4): 1033-1049; https://doi.org/10.1016/j.chempr.2021.01.007

[9] Zhao Y, Han Z, Gao G, et al., Adv. Funct. Mater., 2021, 31(38): 2104976; https://doi.org/10.1002/adfm.202104976

[10] Ye L, Han C, Ma Z, et al., Chem. Eng. J., 2017, 307: 311-318; https://doi.org/10.1016/j.cej.2016.08.102

[11] Zheng X, Zeng W, Gao F, et al., Appl. Surf. Sci., 2025: 162634; https://doi.org/10.1016/j.apsusc.2025.162634

[12] Xu J, Zhang X, Chen X, et al., Inorg. Chem., 2024, 63(38): 17937-17945; https://doi.org/10.1021/acs.inorgchem.4c03268

[13] Xia P, Cao S, Zhu B, et al., Angew. Chem. Int. Ed, 2020, 59(13): 5218-5225; https://doi.org/10.1002/anie.201916012

[14] He F, Zhu B, Cheng B, et al., Appl. Catal. B-Environ, 2020, 272: 119006; https://doi.org/10.1016/j.apcatb.2020.119006

[15] Fu J, Xu Q, Low J, et al., Appl. Catal. B-Environ, 2019, 243: 556-565; https://doi.org/10.1016/j.apcatb.2018.11.011

[16] Song W, Chong K C, Qi G, et al., J. Am. Chem. Soc., 2024, 146(5): 3303-3314; https://doi.org/10.1021/jacs.3c12073

[17] Shen L, Zhou X, Zhang C, et al., J. Food Biochem., 2019, 43(8): e12931; https://doi.org/10.1111/jfbc.12931

[18] Chao Y, Pang J, Bai Y, et al., Food Chem., 2020, 320: 126666; https://doi.org/10.1016/j.foodchem.2020.126666

[19] Liu H, Li P, Qiu F, et al., Food Bioprod. Process., 2020, 123: 177-187; https://doi.org/10.1016/j.fbp.2020.06.018

[20] Yuan J, Zhu Y, Wang J, et al., Food Bioprod. Process., 2021, 126: 293-304; https://doi.org/10.1016/j.fbp.2021.01.004

[21] Zhihua L, Xue Z, Huang X, et al.,Food Chem., 2021, 335: 127646; https://doi.org/10.1016/j.foodchem.2020.127646

[22] Bai M, Li C, Cui H, et al., Lwt, 2021, 146: 111394; https://doi.org/10.1016/j.lwt.2021.111394

[23] Wang X, Pan Y, Wang X, et al., Ind. Crops Prod., 2022, 189: 115863; https://doi.org/10.1016/j.indcrop.2022.115863

[24] Yin L, You T, Arslan M, et al., Food Chem., 2023, 429: 136834; https://doi.org/10.1016/j.foodchem.2023.136834

[25] Javed M, Huang H, Ma Y, et al., Food Chem., 2024, 438: 137948; https://doi.org/10.1016/j.foodchem.2023.137948

[26] Zhang Y, Guo S, Xu X, et al., Appl. Surf. Sci., 2020, 504: 144291; https://doi.org/10.1016/j.apsusc.2019.144291

[27] Luo L, Liu X, Ma S, et al., Food Chem., 2020, 322: 126778; https://doi.org/10.1016/j.foodchem.2020.126778

[28] Liu S, Meng S, Wang M, et al., Food Chem., 2023, 410: 135450; https://doi.org/10.1016/j.foodchem.2023.135450

[29] Shu J, Tang D., Anal. Chem, 2019, 92(1): 363-377; https://doi.org/10.1021/acs.analchem.9b04199

[30] Duan N, Chang B, Zhang H, et al., Int. J. Food Microbiol, 2016, 218: 38-43; https://doi.org/10.1016/j.ijfoodmicro.2015.11.006

[31] Wang L, Tang G, Liu S, et al., Chem. Eng. J., 2022, 428: 131338; https://doi.org/10.1016/j.cej.2021.131338

[32] Ren M, Fakayode O A, Kong F, et al., Ind. Crops Prod., 2023, 197: 116653; https://doi.org/10.1016/j.indcrop.2023.116653

[33] Zhao Z, Zhang W, Liu W, et al., Sci. Total Environ., 2020, 742: 140642; https://doi.org/10.1016/j.scitotenv.2020.140642

[34] Lv X, Wei W, Wang H, et al., Appl. Catal. B-Environ, 2020, 264: 118521; https://doi.org/10.1016/j.apcatb.2019.118521

[35] Tian S, Peng C, Dong J, et al., ACS Catal., 2021, 11(9): 4946-4954; https://doi.org/10.1021/acscatal.1c00455

[36] Li H J W, Zhou H, Chen K, et al., Sol. RRL, 2020, 4(8): 1900416; https://doi.org/10.1002/solr.201900416

[37] Kim E J, Shin J, Bak J, et al., Appl. Catal. B-Environ, 2021, 280: 119433; https://doi.org/10.1016/j.apcatb.2020.119433

[38] Liu H, Yu J, Chen Y, et al., ACS Appl. Mater. Interfaces, 2019, 12(2): 2362-2369; https://doi.org/10.1021/acsami.9b17216

[39] Ji H, Fei T, Zhang L, et al., Appl. Surf. Sci., 2018, 457: 1142-1150; https://doi.org/10.1016/j.apsusc.2018.06.134

[40] Im K, Heo J H, Im S H, et al., Chem. Eng. J., 2017, 330: 698-705;
https://doi.org/10.1016/j.cej.2017.07.160

[41] Du X, Du W, Sun J, et al., Food Chem., 2022, 385: 132731;
https://doi.org/10.1016/j.foodchem.2022.132731

[42] Meng S, Liu D, Li Y, et al., J. Agric. Food. Chem., 2022, 70(42): 13583-13591;
https://doi.org/10.1021/acs.jafc.2c05910

[43] Lai J, Ding L, Liu Y, et al., Food Chem., 2023, 423: 136285;
https://doi.org/10.1016/j.foodchem.2023.136285

[44] Dai Y, Peng W, Ji Y, et al., J. Food Sci., 2024, 89(11): 8022-8035;
https://doi.org/10.1111/1750-3841.17398

[45] Ma M, Huang Z, Doronkin D E, et al., Appl. Catal. B-Environ, 2022, 300: 120695;
https://doi.org/10.1016/j.apcatb.2021.120695